



HAL
open science

Cost-Effective Estimation of Vehicle Lateral Tire-Road Forces and Sideslip Angle via Nonlinear Sampled-Data Observers: Theory and Experiments

Anh-Tu Nguyen, Luciano Frezzatto, Thierry-Marie Guerra, Sébastien Delprat

► **To cite this version:**

Anh-Tu Nguyen, Luciano Frezzatto, Thierry-Marie Guerra, Sébastien Delprat. Cost-Effective Estimation of Vehicle Lateral Tire-Road Forces and Sideslip Angle via Nonlinear Sampled-Data Observers: Theory and Experiments. IEEE/ASME Transactions on Mechatronics, In press, 10.1109/TMECH.2024.3382777 . hal-04553950

HAL Id: hal-04553950

<https://hal.science/hal-04553950>

Submitted on 22 Apr 2024

HAL is a multi-disciplinary open access archive for the deposit and dissemination of scientific research documents, whether they are published or not. The documents may come from teaching and research institutions in France or abroad, or from public or private research centers.

L'archive ouverte pluridisciplinaire **HAL**, est destinée au dépôt et à la diffusion de documents scientifiques de niveau recherche, publiés ou non, émanant des établissements d'enseignement et de recherche français ou étrangers, des laboratoires publics ou privés.

Cost-Effective Estimation of Vehicle Lateral Tire-Road Forces and Sideslip Angle via Nonlinear Sampled-Data Observers: Theory and Experiments

Anh-Tu Nguyen*, *Senior Member, IEEE*, Luciano Frezzatto, Thierry-Marie Guerra, Sébastien Delprat

Abstract—This paper proposes a cost-effective method to jointly estimate the vehicle sideslip angle and lateral tire-road forces, which are crucial to improve the stability and performance of vehicle control systems. This method only requires the information from onboard sensors, readily available on mass-production vehicles. In particular, we consider the case of sampled *asynchronous* measurements, *i.e.*, the vehicle sensor signals used for observer design are transmitted at *arbitrary* and *distinct* times in a certain window bound over the vehicle networked control system. To this end, we propose a new data-sampled observer design, where the asynchronous phenomenon caused by the sampling process is explicitly taken into account via a linear parameter-varying (LPV) framework. Based on an augmented Lyapunov-Krasovskii functional and specific relaxation techniques, the observer design conditions are derived to guarantee an \mathcal{L}_2 -gain performance for the discrete-continuous estimation error dynamics and a maximum allowable sampling period. The observer design is recast as a convex optimization problem, subject to linear matrix inequality (LMI) constraints, which can be efficiently resolved through conventional numerical solvers. The proposed sampled-data observer is experimentally evaluated with an autonomous vehicle under several dynamic driving scenarios, performed on a real test track.

Index Terms—Vehicle dynamics, tire-road forces, sideslip angle, sampled-data observers, aperiodic measurements.

I. INTRODUCTION

Safety and comfort stand out as the utmost priorities when developing advanced driver assistance systems (ADAS) for intelligent vehicles (IVs) [1]. The effectiveness and stability of vehicle control systems significantly rely on real-time information concerning various vehicle states, particularly sideslip angle and tire-road forces [2]–[4]. Precise knowledge of these variables significantly enhances the feedback control performance as well as the capacity to predict real-time tire-road friction and potential vehicle trajectories, which plays a critical role to improve the ADAS control performance [5]–[7]. Unfortunately, obtaining accurate information regarding the vehicle sideslip angle and tire-road forces in mass-production vehicles poses challenges due to the high costs and associated practical limitations [2]. Consequently, it becomes essential to employ alternative methodologies, such as observation or estimation, to effectively determine these vehicle variables.

Extensive research efforts have been dedicated to developing vehicle state estimation methods with a focus on utilizing cost-effective vehicle sensors [2]. To this end, various tire-road force models have been exploited, including linear tire models, Brush tire models, Dugoff tire models and Pacejka models [3], [5]. Under normal driving conditions, using the well-known bicycle model and linear tire models, Luenberger observers have been widely developed to estimate the vehicle lateral speed or the sideslip angle [8], [9]. Under similar vehicle modeling assumptions, a fuzzy adaptive robust cubature Kalman filter (CKF) was proposed in [10] to recover the information of the sideslip angle and the tire cornering stiffness. Based on the Brush tire model, a nonlinear observer has been proposed to estimate the sideslip angle in [11]. A robust adaptive observer methodology was proposed in [12] to estimate simultaneously the friction coefficient and vehicle slip angle using the lateral acceleration and the tire-aligning moment. Based on test data, the authors in [13] proposed a modified version of the Brush tire model to develop a method, combining auxiliary particle filter (APF) and iterated extended Kalman filter (EKF) with iteration, to estimate the tire slip angle and the tire-road friction coefficient with non-Gaussian noise. Zhang *et al.* [14] presented an estimation framework based on an improved Brush tire model and a modified square-root CKF to directly identify the road friction coefficients. The Dugoff tire models have been leveraged to develop algorithms to estimate the sideslip angle and/or lateral forces or the tire-road friction coefficient using an algebraic filtering technique [15], a Takagi-Sugeno fuzzy observer design [16], a sliding mode observer combined with an EKF [17]. In particular, Doumiati *et al.* [18] experimentally demonstrated with road results that unscented Kalman filters (UKFs) can provide a significantly better estimation performance for vehicle sideslip angle and tire-road forces than EKFs with respect to road variations. A modified Dugoff model was used in [19] to develop a dual linear time-varying Kalman filter to estimate the sideslip angle and the cornering stiffness. Based on Pacejka models, various Kalman filter-based algorithms have been also proposed for vehicle estimation, *e.g.*, [20]–[22]. Especially, Wang *et al.* [23] developed an adaptive fault-tolerant EKF, which can efficiently mitigate the impact of partial loss of sensor data, parameter perturbations, and state mutation on estimation accuracy. Many other nonlinear estimation techniques based on other different tire-road models such as LuGre tire models, Burchhardt tire models, UniTire tire models, etc. can be documented in [2]. Unfortunately, most of these estimation

A.-T. Nguyen, T.-M. Guerra and S. Delprat are with the LAMIH laboratory, UMR CNRS 8201, Université Polytechnique Hauts-de-France, Valenciennes, France. A.-T. Nguyen and S. Delprat are also with the INSA Hauts-de-France, Valenciennes, France (e-mail: tnguyen@uphf.fr).

L. Frezzatto is with the Universidade Federal de Minas Gerais, Belo Horizonte, Brazil (e-mail: lfrezzatto@ufmg.br).

techniques require a precise knowledge about the tire model parameters and properties. Hence, extensive research efforts have been devoted to identifying the tire model parameters [24], [25]. However, such an identification task still remains challenging to reconstruct the tire characteristics under various driving conditions [5], [24]. To overcome this major drawback, taking into account state constraints, Strano *et al.* [26] developed a constrained UKF for sideslip angle estimation without *a priori* knowledge of tire characteristics. An IMM-based estimator was proposed in [27] to estimate the tire slip angle under various road conditions without tire–road information. To avoid the dependency on the vehicle and tire models, machine learning and data-driven estimation approaches have been also exploited, *e.g.*, [28], [29]. However, the related training processes are usually based on reference data which are typically not available from mass-production vehicles [30].

We can see that Kalman filtering techniques have occupied a large body of literature on the estimation of sideslip angle and/or tire-road forces [2]. The main reason is due to their ability to cope with the nonlinearities, parameter uncertainties and disturbances/noises involved in the vehicle systems. Kalman filters typically exhibit effective performance when a precise vehicle model is accessible [30]. Nonetheless, if the propagation of errors cannot be sufficiently captured, the EKF performance may decline and potentially lead to instability [12]. EKFs based on kinematic vehicle models can improve the robustness with respect to vehicle parameter variations, *e.g.*, tire-road parameters, vehicle mass, inertia, etc. [31], albeit with a trade-off of slightly noisier estimation results, due to their strong dependency on the sensor quality. Moreover, despite some practical guidelines [30], the tuning efforts related to EKF-based estimation algorithms still remain time-consuming. Furthermore, most of the existing approaches essentially focus on the practical estimation performance without paying special attention on the proofs of convergence and robustness. Indeed, due to the complexity of the vehicle system modeling, there is still a lack of literature on the joint estimation sideslip angle and/or tire-road forces with theoretical guarantees. Recently, based on Lyapunov stability theory, an asymptotic sampled-data observer was proposed in [8] to estimate the lateral velocity by exploiting only the knowledge of sparse yaw rate samples. However, this method is only effective in the presence of sufficiently bounded driver maneuvers. Moreover, the vehicle lateral tire-road forces cannot be estimated with [8]. Jeon *et al.* [32] also developed an interesting neuro-adaptive observer to provide asymptotically stable estimation of the vehicle state and the neural network (NN) weights of the learned tire model. However, appropriate initial conditions for the NN weights must be obtained to ensure the convergence. Moreover, only simulation results were presented in [8], [32]. Hence, further experimental tests should be performed to verify the practical performance of these observer schemes.

Motivated by the above practical and theoretical estimation issues, this paper presents a new nonlinear observer method to jointly estimate the vehicle sideslip angle and lateral tire-road forces. The cost-effective nature of the observer scheme hinges on the fact that only information from readily available onboard sensors is necessary to estimate these crucial

vehicle variables. However, this feature poses a significant challenge, *i.e.*, the well-known matching condition [9] is not verified to reconstruct the lateral tire-road forces, considered as the unknown inputs (UIs) of the vehicle system. Hence, standard unknown input observers (UIOs) with decoupling-based approaches [9], [16], [33] cannot be applied in this case. In particular, for observer design we consider sampled asynchronous measurements gathered from vehicle sensors, which can practically take place at arbitrary instants in a certain window with upper and lower limits. It is emphasized that the existing estimation approaches, *e.g.*, EKFs/UKFs or other nonlinear observers previously discussed, require the sensor data to be transmitted at every fixed (and usually very small [31]) sampling period. In specific situations where the output is solely accessible at distinct time instants as in IVs networked control systems [8], [34], these traditional estimation approaches need to be properly “redesigned” for digital implementation [35]. Note also that using an exact or approximate discrete-time models of nonlinear systems for observer design cannot explicitly take into account the perturbations in between two consecutive sampling instants [36]. To avoid this technical issue, we directly use a continuous-time nonlinear model to synthesize a sampled-data observer for vehicle estimation, resulting in a continuous-discrete observer design. The asynchronous phenomenon caused by the sampling process is explicitly taken into account in the observer design using a polytopic linear parameter-varying (LPV) framework. An augmented Lyapunov-Krasovskii functional together with specific relaxation techniques are leveraged to derive the design conditions while guaranteeing an \mathcal{L}_2 -gain performance for the estimation error dynamics and a maximum allowable sampling period (MASP). The discrete-continuous observer design is recast as an LMI-based optimization problem, which can be efficiently resolved using common solvers [37]. Specifically, our main contributions are summarized as follows.

- We propose an estimation method to jointly estimate the sideslip angle and tire-road forces using only sensors, commonly available on mass-production vehicles.
- Based on a continuous-time nonlinear vehicle model, a new data-sampled observer is proposed, taking into account the discrete-time nature of the sampled *asynchronous* measurements from vehicle sensors.
- The estimation convergence and \mathcal{L}_2 -gain performance are *theoretically* guaranteed via Lyapunov-Krasovskii stability theory. The continuous-discrete observer design is recast as an LMI-based optimization problem.
- The proposed data-sampled observer is experimentally validated under several driving scenarios, performed with the test facilities shown in Fig. 1.

It is emphasized that the joint estimation of sideslip angle and tire-road forces, considering asynchronously sampled measurements from common vehicle sensors with theoretical performance guarantees, has not been observed in the literature.

Notation. \mathbb{N}_+ is the set of positive integers, \mathbb{R} is the set of real numbers, \mathbb{R}_+ is the set of positive real numbers, $\mathbb{R}^{m \times n}$ is the set of all $m \times n$ real matrices, and $\mathcal{I}_q \equiv \{1, \dots, q\} \subset \mathbb{N}_+$. For a vector \mathbf{x} , we denote $\|\mathbf{x}\| = \sqrt{\mathbf{x}^\top \mathbf{x}}$. For a matrix X ,



Fig. 1. Experimental facilities. (a) INSA-LAMIH autonomous vehicle, (b) Gyrovia test track in Valenciennes, France.

its transpose is denoted by X^\top , $X \succ 0$ means that X is positive definite, and $\text{He}(X) = X + X^\top$. $\text{blkdiag}(X_1, X_2)$ denotes a block-diagonal matrix composed of two matrices X_1 and X_2 . We denote I as an identity matrix of appropriate dimension. The symbol \star represents the transposed terms in a symmetric matrix. $\lambda_{\min}(\cdot)$ denotes the minimum eigenvalue of a real symmetric matrix. The arguments of functions are omitted when convenient.

II. VEHICLE MODELING

This section reviews the key elements of vehicle modeling for nonlinear observer design. The parameters of the INSA-LAMIH autonomous vehicle are given in Table I.

TABLE I
VEHICLE NOMENCLATURE.

Parameter	Description	Value
v_y	Vehicle lateral speed	-
v_x	Vehicle longitudinal speed	-
y_r	Yaw rate	-
δ	Front wheel steering angle	-
T_w	Longitudinal wheel torque	-
m_v	Vehicle mass	1077 [kg]
C_f	Front cornering stiffness	47135 [N/rad]
C_r	Rear cornering stiffness	56636 [N/rad]
l_f	Distance from gravity center to front axle	1.08 [m]
l_r	Distance from gravity center to rear axle	1.24 [m]
I_z	Vehicle yaw moment of inertia	1442 [kgm ²]
R_t	Tires effective rolling radius	0.26 [m]
ρ_a	Air density	1.23 [kg/m ³]
C_{dy}	Lateral drag coefficient	0.35 [-]
C_{dx}	Longitudinal drag coefficient	0.32 [-]
A_{fy}	Lateral frontal area	2.01 [m ²]
A_{fx}	Longitudinal frontal area	1.97 [m ²]

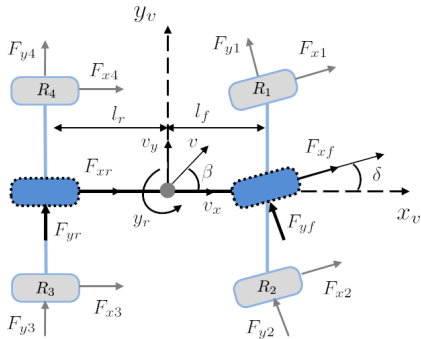


Fig. 2. Diagram of a 2-DoF vehicle model.

We consider a bicycle vehicle model with two degrees of freedom, as shown in Fig. 2. In scenarios of typical driving, assuming small angles and no longitudinal slip, the nonlinear dynamics of the vehicle can be expressed as follows [9], [38]:

$$\begin{aligned} m_v(\dot{v}_x - y_r v_y) &= \frac{T_w}{R_t} - F_{ax} \\ m_v(\dot{v}_y + y_r v_x) &= F_{yf} + F_{yr} - F_{ay} \\ I_z \dot{y}_r &= l_f F_{yf} - l_r F_{yr} \end{aligned} \quad (1)$$

where $F_{ax} = 0.5C_{dx}\rho_a A_{fx}v_x^2$ is the longitudinal aerodynamic drag force, $F_{ay} = 0.5C_{dy}\rho_a A_{fy}v_y^2$ is the lateral aerodynamic drag force when cornering, and F_{yf} and F_{yr} are the lateral tires forces on front and rear tires. Experimental findings show that F_{yf} and F_{yr} are nonlinearly related to slip angles, except for small angles where they have a linear relationship [38]. Then, the lateral tire-road forces can be described as

$$\begin{aligned} F_{yf} &= 2C_f(1 + W_f\Delta(\alpha_f))\alpha_f \\ F_{yr} &= 2C_r(1 + W_r\Delta(\alpha_r))\alpha_r \end{aligned} \quad (2)$$

where the sideslip angles α_f and α_r are given by

$$\alpha_f = \delta - \frac{v_y + l_f r}{v_x}, \quad \alpha_r = \frac{l_r r - v_y}{v_x}. \quad (3)$$

The term $\Delta(\alpha_f)$ (respectively $\Delta(\alpha_r)$) represents the nonlinear part of F_{yf} (respectively F_{yr}). Since $\Delta(\alpha_q)$, for $q \in \{f, r\}$, is considered as uncertainties of the lateral tires forces, it can be normalized as $-1 \leq \Delta(\alpha_q) \leq 1$. Moreover, W_q , for $q \in \{f, r\}$, is a weight used for normalization for which $2C_q(1 + W_q)$ and $2C_q(1 - W_q)$, for $q \in \{f, r\}$, are respectively the upper and lower bounds of the slopes of the lateral forces characteristics, *i.e.*,

$$2C_q(1 - W_q) \leq \frac{\partial}{\partial \alpha_q} F_{yq} \leq 2C_q(1 + W_q), \quad q \in \{f, r\}.$$

Let us denote $F_f = \Delta(\alpha_f)\alpha_f$ and $F_r = \Delta(\alpha_r)\alpha_r$ as modeling uncertainties related to the lateral tires forces. The uncertain lateral tires forces in (2) can be reformulated as

$$\begin{aligned} F_{yf} &= 2C_f\alpha_f + 2C_fW_fF_f \\ F_{yr} &= 2C_r\alpha_r + 2C_rW_rF_r. \end{aligned} \quad (4)$$

From (1), (3) and (4), the vehicle nonlinear dynamics can be represented in the state-space form as

$$\dot{\mathbf{x}} = f(\mathbf{x}) + \mathbf{B}\mathbf{u} + \mathbf{D}\mathbf{d} \quad (5)$$

where $\mathbf{x} = [v_y \quad y_r \quad v_x]^\top$ is the vehicle state vector, $\mathbf{u} = [\delta \quad T_w]^\top$ is the *known* control input, and $\mathbf{d} = [F_f \quad F_r]^\top$ is the *unknown* uncertainty input. The nonlinear function $f(\mathbf{x})$ and the state-space matrices \mathbf{B} and \mathbf{D} in (5) are given by

$$\begin{aligned} f(\mathbf{x}) &= \begin{bmatrix} a_{12} \frac{y_r}{v_x} - a_{11} \frac{v_y}{v_x} - y_r v_x - C_y v_y^2 \\ a_{21} \frac{v_y}{v_x} - a_{22} \frac{y_r}{v_x} \\ y_r v_y - C_x v_x^2 \end{bmatrix} \\ \mathbf{B} &= \begin{bmatrix} \frac{2C_f}{m_v} & 0 \\ \frac{2C_f l_f}{I_z} & 0 \\ 0 & \frac{1}{m_v R_t} \end{bmatrix}, \quad \mathbf{D} = \begin{bmatrix} \frac{2C_f W_f}{I_z} & \frac{2C_r W_r}{I_z} \\ 0 & 0 \end{bmatrix} \end{aligned}$$

with

$$\begin{aligned} a_{11} &= \frac{2(C_f + C_r)}{m_v}, & a_{12} &= \frac{2(C_r l_r - C_f l_f)}{m_v} \\ a_{21} &= \frac{2(C_r l_r - C_f l_f)}{I_z}, & a_{22} &= \frac{2(C_f l_f^2 + C_r l_r^2)}{I_z} \\ C_x &= \frac{C_{dx} \rho_a A_{fx}}{2m_v}, & C_y &= \frac{C_{dy} \rho_a A_{fy}}{2m_v}. \end{aligned}$$

As in practice, while the yaw rate y_r and the vehicle speed v_x can be measured inexpensively, measuring the lateral speed v_y or the sideslip angle β remains unattainable for commercial vehicle applications due to sensor cost reasons [16]. Moreover, within the IVs network control system, the onboard sensor signals are transmitted through a common digital communication network, and are accessible only at discrete-time instants [8], [34]. Hence, the output of system (5) is given by

$$\mathbf{y}_k = C \mathbf{x}_k, \quad C = \begin{bmatrix} 0 & 1 & 0 \\ 0 & 0 & 1 \end{bmatrix} \quad (6)$$

where \mathbf{y}_k is the sample of $\mathbf{y}(t)$ taken at the sampling instants $\{t_0, t_1, t_2, \dots\}$. We consider sampled asynchronous measurements that occur at arbitrary times in a certain window such that the next sampling instant is defined as

$$t_{k+1} = \{t \in \mathbb{R}_+ : t > t_k \text{ and } t - t_k \leq T_m\} \quad (7)$$

where $T_m > 0$ is the maximum allowable sampling period.

From the vehicle nonlinear dynamics (5) and the output (6) with the asynchronous sampling process (7), we propose in Section III a new sampled-data observer design. Note also that $\beta = \text{atan}\left(\frac{v_y}{v_x}\right)$ [38], then, estimating the lateral speed v_y is equivalent to estimating the sideslip angle β .

III. NONLINEAR SAMPLED-DATA OBSERVER DESIGN

This section first formulates the estimation problem of lateral tire-road forces and sideslip angle. Then, we present LMI-based conditions to design the related \mathcal{L}_2 -gain sampled-data nonlinear observer for joint estimation purposes.

A. Problem Formulation

For generality, the vehicle system (5) with the output (6) is reconsidered in the following more general form:

$$\begin{aligned} \dot{\mathbf{x}}(t) &= f(\mathbf{x}(t)) + B\mathbf{u}(t) + D\mathbf{d}(t) \\ \mathbf{y}_k &= C\mathbf{x}_k \end{aligned} \quad (8)$$

with $\mathbf{x} \in \mathbb{R}^{n_x}$, $\mathbf{u} \in \mathbb{R}^{n_u}$, $\mathbf{d} \in \mathbb{R}^{n_d}$ and $\mathbf{y}_k \in \mathbb{R}^{n_y}$. For observer design, we consider the following assumption for system (8).

Assumption 1. The matrix D is of full column rank, *i.e.*, $\text{rank}(D) = n_d$.

Remark 1. Without any loss of generality, Assumption 1 can be obtained by removing redundant components of $\mathbf{d}(t)$. In contrast to most of existing results on UIO design [16], [33], here the well-known matching condition, *i.e.*, $\text{rank}(CD) = \text{rank}(D)$ is not required. Note that such a matching condition is not verified for the vehicle system (5). In particular, no *a priori* information on $\mathbf{d}(t)$ is required as for proportional-integral observer designs [39].

To jointly estimate the state \mathbf{x} and the unknown input \mathbf{d} , the following nonlinear sampled-data observer is considered:

$$\begin{aligned} \dot{\hat{\mathbf{x}}} &= f(\hat{\mathbf{x}}) + B\mathbf{u} + D\hat{\mathbf{d}} + L(\mathbf{h}_k)(\mathbf{y}_k - \hat{\mathbf{y}}_k) \\ \dot{\hat{\mathbf{z}}} &= -KD\hat{\mathbf{z}} - K(f(\hat{\mathbf{x}}) + B\mathbf{u} + DK\hat{\mathbf{x}}) \\ \hat{\mathbf{y}}_k &= C\hat{\mathbf{x}}_k, \quad \hat{\mathbf{d}} = \hat{\mathbf{z}} + K\hat{\mathbf{x}} \end{aligned} \quad (9)$$

where $\hat{\chi}$ is the estimate of χ , for $\chi \in \{\mathbf{x}, \mathbf{y}_k, \mathbf{d}, \mathbf{z}\}$. The estimation error corresponding to any variable χ is given by $\mathbf{e}_\chi = \chi - \hat{\chi}$. The intermediate variable \mathbf{z} in the observer (9) is defined as

$$\mathbf{z} = \mathbf{d} - K\mathbf{x} \quad (10)$$

where the gain matrix K is predefined as

$$K = \tau D^\top \quad (11)$$

with $\tau > 0$. The parameter-dependent observer gain $L(\mathbf{h}_k) \in \mathbb{R}^{n_x \times n_y}$ is to be designed, and $\mathbf{h}_k = \mathbf{h}(t_k)$ is the scheduling parameter sampled at instant k . We have from (10) that

$$\mathbf{d} = \mathbf{z} + K\mathbf{x}. \quad (12)$$

It follows from (9) and (12) that

$$\mathbf{e}_d = \mathbf{e}_z + K\mathbf{e}_x. \quad (13)$$

Then, the estimation error dynamics can be obtained from (5), (9) and (13) as

$$\begin{aligned} \dot{\mathbf{e}}_x &= f(\mathbf{x}) - f(\hat{\mathbf{x}}) + D(\mathbf{e}_z + K\mathbf{e}_x) - L(\mathbf{h}_k)C\mathbf{e}_{x_k} \\ \dot{\mathbf{e}}_z &= \dot{\mathbf{d}} - K(f(\mathbf{x}) - f(\hat{\mathbf{x}}) + D\mathbf{e}_z + DK\mathbf{e}_x) \end{aligned} \quad (14)$$

where \mathbf{e}_{x_k} is the sampled value of \mathbf{e}_x at instant k , and

$$f(\mathbf{x}) - f(\hat{\mathbf{x}}) = \begin{bmatrix} \left(a_{12} \left(\frac{y_r}{v_x} - \frac{\hat{y}_r}{\hat{v}_x} \right) - a_{11} \left(\frac{v_y}{v_x} - \frac{\hat{v}_y}{\hat{v}_x} \right) \right) \\ \left(-y_r v_x - \hat{y}_r \hat{v}_x \right) - C_y (v_y^2 - \hat{v}_y^2) \\ a_{21} \left(\frac{v_y}{v_x} - \frac{\hat{v}_y}{\hat{v}_x} \right) - a_{22} \left(\frac{y_r}{v_x} - \frac{\hat{y}_r}{\hat{v}_x} \right) \\ y_r v_y - \hat{y}_r \hat{v}_y - C_x (v_x^2 - \hat{v}_x^2) \end{bmatrix}. \quad (15)$$

Due to the physical limitations related to the driving conditions performed with the test track, depicted in Fig. 1(b), the vehicle state variables are bounded as [29]

$$\mathbf{x} \in \mathcal{D} = \{v_y \in [v_y, \bar{v}_y], y_r \in [y_r, \bar{y}_r], v_x \in [v_x, \bar{v}_x]\}$$

with $\bar{v}_y = -v_y = 1.5$ [m/s], $\bar{y}_r = -y_r = 1.1$ [rad/s], $v_x = 1.5$ [m/s], and $\bar{v}_x = 20$ [m/s]. For observer design, to obtain a tractable form with reduced complexity of $f(\mathbf{x}) - f(\hat{\mathbf{x}})$, we adopt the following variable changes and first-order Taylor approximations [40]:

$$\begin{aligned} \frac{1}{v_x} &= \frac{1}{v_0} + \frac{1}{v_1} \xi, & \frac{1}{\hat{v}_x} &= \frac{1}{v_0} + \frac{1}{v_1} \hat{\xi} \\ v_x &\simeq v_0 \left(1 - \frac{v_0}{v_1} \xi \right), & v_x^2 &\simeq v_0^2 \left(1 - 2 \frac{v_0}{v_1} \xi \right) \\ \hat{v}_x &\simeq v_0 \left(1 - \frac{v_0}{v_1} \hat{\xi} \right), & \hat{v}_x^2 &\simeq v_0^2 \left(1 - 2 \frac{v_0}{v_1} \hat{\xi} \right) \\ v_0 &= \frac{2v_x \bar{v}_x}{v_x + \bar{v}_x}, & v_1 &= \frac{2v_x \bar{v}_x}{v_x - \bar{v}_x}. \end{aligned} \quad (16)$$

The new variables $\xi \in [-\bar{\xi}, \bar{\xi}]$ and $\hat{\xi} \in [-\bar{\xi}, \bar{\xi}]$, with $\bar{\xi} = -\underline{\xi} = 1$, are employed to characterize the variations of v_x and \hat{v}_x ,

respectively, within the range defined by their lower limit \underline{v}_x and upper limit \bar{v}_x . Then, using (16) it follows that

$$\begin{aligned} v_x - \hat{v}_x &\simeq -\frac{2v_0}{v_1}e_\xi, & y_r v_y - \hat{y}_r \hat{v}_y &= y_r e_{v_y} + \hat{v}_y e_{y_r} \\ v_x^2 - \hat{v}_x^2 &\simeq -\frac{2v_0^3}{v_1}e_\xi, & v_y^2 - \hat{v}_y^2 &= (v_y + \hat{v}_y)e_{v_y} \\ y_r v_x - \hat{y}_r \hat{v}_x &\simeq -\frac{v_0^2}{v_1}y_r e_\xi + v_0 \left(1 - \frac{v_0}{v_1}\hat{\xi}\right) e_{y_r} \\ \frac{\vartheta}{v_x} - \frac{\hat{\vartheta}}{\hat{v}_x} &\simeq \left(\frac{1}{v_0} + \frac{1}{v_1}\hat{\xi}\right) e_\vartheta + \frac{1}{v_1}\vartheta e_\xi, & \vartheta &\in \{y_r, v_y\}. \end{aligned} \quad (17)$$

Using the expressions in (17), we can rewrite (15) as

$$\begin{aligned} f(\mathbf{x}) - f(\hat{\mathbf{x}}) &= F(\mathbf{x}, \hat{\mathbf{x}})\mathbf{e}_x \\ &= (F_0 + \hat{v}_y F_1 + y_r F_2 + \hat{\xi} F_3 + v_y F_4)\mathbf{e}_x \end{aligned} \quad (18)$$

with

$$\begin{aligned} F_0 &= \begin{bmatrix} -\frac{a_{11}}{v_0} & \frac{a_{12}}{v_0} - v_0 & 0 \\ \frac{a_{21}}{v_0} & -\frac{a_{22}}{v_0} & 0 \\ 0 & 0 & -C_x v_0 \end{bmatrix} \\ F_1 &= \begin{bmatrix} -C_y & 0 & 0 \\ 0 & 0 & 0 \\ 0 & -\frac{v_1}{v_0^2} & 0 \end{bmatrix}, & F_2 &= \begin{bmatrix} 0 & 0 & \frac{v_0^2 + a_{12}}{v_1} \\ 0 & 0 & -\frac{a_{22}}{v_1} \\ -\frac{v_1}{v_0} & 0 & 0 \end{bmatrix} \\ F_3 &= \begin{bmatrix} -\frac{a_{11}}{v_1} & \frac{v_0^2 + a_{12}}{v_1} & 0 \\ \frac{a_{21}}{v_1} & -\frac{a_{22}}{v_1} & 0 \\ 0 & 0 & 0 \end{bmatrix}, & F_4 &= \begin{bmatrix} -C_y & 0 & -\frac{a_{11}}{v_1} \\ 0 & 0 & \frac{a_{21}}{v_1} \\ 0 & 0 & 0 \end{bmatrix}. \end{aligned}$$

Note from (18) that the nonlinear matrix $F(\mathbf{x}, \hat{\mathbf{x}})$ linearly depends on the variables \hat{v}_y , y_r , $\hat{\xi}$ and v_y . Then, using the well-known sector nonlinearity approach [41, Chapter 2], we can rewrite $f(\mathbf{x}) - f(\hat{\mathbf{x}})$ in the following LPV polytopic form:

$$\begin{aligned} f(\mathbf{x}) - f(\hat{\mathbf{x}}) &= (F_0 + r_1(t)\bar{v}_y F_1 + (1 - r_1(t))\underline{v}_y F_1 \\ &\quad + r_2(t)\bar{y}_r F_2 + (1 - r_2(t))\underline{y}_r F_2 \\ &\quad + r_3(t)\bar{\xi} F_3 + (1 - r_3(t))\underline{\xi} F_3 \\ &\quad + r_4(t)\bar{v}_y F_4 + (1 - r_4(t))\underline{v}_y F_4)\mathbf{e}_x \end{aligned} \quad (19)$$

with

$$\begin{aligned} r_1(t) &= \frac{\hat{v}_y(t) - \underline{v}_y}{\bar{v}_y - \underline{v}_y}, & r_2(t) &= \frac{y_r(t) - \underline{y}_r}{\bar{y}_r - \underline{y}_r} \\ r_3(t) &= \frac{\hat{\xi}(t) - \underline{\xi}}{\bar{\xi} - \underline{\xi}}, & r_4(t) &= \frac{v_y(t) - \underline{v}_y}{\bar{v}_y - \underline{v}_y}. \end{aligned}$$

The polytopic expression (19) can be rewritten as

$$f(\mathbf{x}) - f(\hat{\mathbf{x}}) = A(\boldsymbol{\sigma})\mathbf{e}_x = \left(\sum_{i=1}^{16} \sigma_i(t) A_i \right) \mathbf{e}_x \quad (20)$$

where the constant matrices A_i , for $i \in \mathcal{I}_{16}$, are obtained from all possible combinations of the minimum and maximum bounds of \hat{v}_y , y_r , $\hat{\xi}$ and v_y . The nonlinear scalar functions $\sigma_i(t) = \sigma_i(r_1(t), r_2(t), r_3(t), r_4(t))$, for $i \in \mathcal{I}_{16}$, are constructed from the combinations of $r_j(t)$, for $j \in \mathcal{I}_4$, which satisfy the convex sum property [41]

$$\sum_{i=1}^{16} \sigma_i(t) = 1, \quad \sigma_i(t) \geq 0. \quad (21)$$

Using (20), the errors dynamics (14) can be rewritten as

$$\dot{\bar{\boldsymbol{\varepsilon}}} = A_{\bar{\boldsymbol{\varepsilon}}}\bar{\boldsymbol{\varepsilon}} + A_{\bar{\boldsymbol{\varepsilon}}_k}\bar{\boldsymbol{\varepsilon}}_k + D_{\bar{\boldsymbol{\varepsilon}}}\bar{\mathbf{w}} \quad (22)$$

where $\bar{\boldsymbol{\varepsilon}} = [\mathbf{e}_x^\top \quad \mathbf{e}_z^\top]^\top$, $\bar{\mathbf{w}} = \dot{\mathbf{d}}$, and

$$\begin{aligned} A_{\bar{\boldsymbol{\varepsilon}}} &= \begin{bmatrix} A(\boldsymbol{\sigma}) + DK & D \\ -K(A(\boldsymbol{\sigma}) + DK) & -KD \end{bmatrix} \\ A_{\bar{\boldsymbol{\varepsilon}}_k} &= \begin{bmatrix} -L(\mathbf{h}_k)C & 0 \\ 0 & 0 \end{bmatrix}, & D_{\bar{\boldsymbol{\varepsilon}}} &= [0 \quad 1]^\top. \end{aligned}$$

To achieve an exponential convergence of the estimation errors, we perform the following variable change:

$$\boldsymbol{\varepsilon}(t) = e^{\alpha t} \bar{\boldsymbol{\varepsilon}}(t) \quad (23)$$

where $\alpha > 0$ is a predefined decay rate. Hence, the transformed error system can be obtained from (22) and (23) as

$$\dot{\boldsymbol{\varepsilon}}(t) = A_\varepsilon \boldsymbol{\varepsilon}(t) + A_{\varepsilon_k} \boldsymbol{\varepsilon}_k + D_\varepsilon \mathbf{w}(t) \quad (24)$$

with $A_\varepsilon = A_{\bar{\boldsymbol{\varepsilon}}} + \alpha I$, $A_{\varepsilon_k} = e^{\alpha(t-t_k)} A_{\bar{\boldsymbol{\varepsilon}}_k}$, and $\mathbf{w} = e^{2\alpha t} \bar{\mathbf{w}}$.

Remark 2. Although v_y is used to define the LPV polytopic form (20), this variable cannot be exploited for implementation of the observer gain $L(\mathbf{h}_k)$ in (9) due to its online unavailability. Hence, the sampled scheduling parameter $\mathbf{h}_k = \mathbf{h}(t_k)$ is only constructed using the measured/estimated variables \hat{v}_y , $\hat{\xi}$ and y_r , i.e., $L(\mathbf{h}_k) = \sum_{i=1}^8 h_i(t_k) L_i$, where $h_i(t_k) = h_i(r_1(t_k), r_2(t_k), r_3(t_k))$, for $i \in \mathcal{I}_8$, are defined from the combinations of $r_j(t_k)$, for $j \in \mathcal{I}_3$. The functions $h_i(t_k)$, for $i \in \mathcal{I}_8$, also satisfy the convex sum property as in (21).

We are now ready to formalize the gain-scheduled sampled-data observer design problem for the nonlinear system (8).

Problem 1. Consider system (8) and the discrete-continuous observer (9). Determine the parameter-dependent observer gain $L(\mathbf{h}_k) \in \mathbb{R}^{n_x \times n_y}$ such that the error dynamics (24) satisfies the following properties.

- (P1). If $\mathbf{w}(t) = 0$, for $\forall t > 0$, the error dynamics (22) is globally exponentially stable.
- (P2). If $\mathbf{w}(t) \neq 0$, for $\forall t > 0$ and for any energy-bounded $\mathbf{w}(t)$, under null initial condition $\boldsymbol{\varepsilon}_0 = 0$, we have

$$\int_{t_0}^t \|\boldsymbol{\varepsilon}(\tau)\|^2 d\tau \leq \rho^2 \int_{t_0}^t \|\mathbf{w}(\tau)\|^2 d\tau, \quad \rho \in \mathbb{R}_+. \quad (25)$$

The following lemmas are useful to design the sampled-data observer (9) for vehicle estimation purposes.

Lemma 1 (Finsler's lemma [37]). Let $\boldsymbol{\zeta} \in \mathbb{R}^n$ and $\mathcal{B} \in \mathbb{R}^{m \times n}$. The following implications are equivalent:

- (i) $\boldsymbol{\zeta}^\top \mathcal{Q} \boldsymbol{\zeta} < 0$, $\forall \boldsymbol{\zeta} \neq 0$ such that $\mathcal{B} \boldsymbol{\zeta} = 0$;
- (ii) $\exists \mathcal{X} \in \mathbb{R}^{n \times m}$ such that $\mathcal{Q} + \mathcal{X} \mathcal{B} + \mathcal{B}^\top \mathcal{X}^\top \prec 0$.

Lemma 2 (Wirtinger's inequality [42]). Given a positive definite matrix R , the following inequality holds for every function $\boldsymbol{\omega}(u)$ continuously differentiable in $[a, b] \rightarrow \mathbb{R}^n$:

$$\int_a^b \dot{\boldsymbol{\omega}}^\top(u) R \dot{\boldsymbol{\omega}}(u) du \geq \frac{1}{b-a} \Omega_1^\top R \Omega_1 + \frac{3}{b-a} \Omega_2^\top R \Omega_2 \quad (26)$$

with

$$\Omega_1 = \boldsymbol{\omega}(b) - \boldsymbol{\omega}(a), \quad \Omega_2 = \boldsymbol{\omega}(b) - \boldsymbol{\omega}(a) - \frac{2}{b-a} \int_a^b \boldsymbol{\omega}(u) du.$$

Remark 3. Note that by discarding the second term on the right-hand side of (26), the resulting condition is equivalent to the well-known Jensen's inequality [42].

B. Gain-Scheduled Sampled-Data Observer Design

The following theorem presents sufficient condition to design a gain-scheduled sampled-data observer (9) such that the properties in Problem 1 can be ensured. For simplicity of notation, let us define $n_\varepsilon = n_x + n_d$. Moreover, we denote

$$U(\mathbf{h}_k) = \sum_{i=1}^8 h_i(t_k) U_i, \quad V(\boldsymbol{\sigma}, \mathbf{h}_k) = \sum_{l=1}^{16} \sum_{m=1}^8 \sigma_l(t) h_m(t_k) V_{lm}.$$

for any matrices of appropriate dimensions U_i and V_{lm} , with $(i, l, m) \in \mathcal{I}_8 \times \mathcal{I}_{16} \times \mathcal{I}_8$.

Theorem 1. Consider system (8), a MASP T_m , and scalars $\tau > 0$, $\alpha > 0$, $\lambda_1, \lambda_2, \lambda_3$, and $\lambda_4 > 0$. If there exist symmetric positive definite matrices $P_1(\mathbf{h}_k)$, $P_3(\mathbf{h}_k)$, $R_1(\mathbf{h}_k)$, $R_2(\mathbf{h}_k)$, $E_1(\mathbf{h}_k)$, $E_3(\mathbf{h}_k)$, $Q(\mathbf{h}_k)$, $S(\mathbf{h}_k) \in \mathbb{R}^{n_\varepsilon \times n_\varepsilon}$, matrices $P_2(\mathbf{h}_k)$, $E_2(\mathbf{h}_k)$, $X_1(\mathbf{h}_k)$, $X_2(\mathbf{h}_k) \in \mathbb{R}^{n_\varepsilon \times n_\varepsilon}$, $N_{ij}(\boldsymbol{\sigma}, \mathbf{h}_k) \in \mathbb{R}^{n_\varepsilon \times n_\varepsilon}$, for $(i, j) \in \mathcal{I}_2 \times \mathcal{I}_5$, $F(\mathbf{h}_k) \in \mathbb{R}^{n_x \times n_x}$, $Z(\mathbf{h}_k) \in \mathbb{R}^{n_x \times n_y}$, $Y_{i2}(\boldsymbol{\sigma}, \mathbf{h}_k) \in \mathbb{R}^{n_x \times n_d}$, $Y_{i4}(\boldsymbol{\sigma}, \mathbf{h}_k) \in \mathbb{R}^{n_d \times n_d}$, for $i \in \mathcal{I}_5$, and a positive scalar ρ such that the following optimization problem is feasible:

$$\min \rho^2 \quad (27)$$

subject to

$$P(\mathbf{h}_k) \succeq 0, \quad R_1(\mathbf{h}_k) \succeq 0, \quad R_2(\mathbf{h}_k) \succeq 0 \quad (28)$$

$$E(\mathbf{h}_k) \succeq 0, \quad Q(\mathbf{h}_k) \succeq 0, \quad S(\mathbf{h}_k) \succeq 0 \quad (29)$$

$$\begin{bmatrix} \Omega + T_m \Psi + \text{He}(\Lambda \Gamma) & \star \\ D_\varepsilon^\top Y^\top & -\rho^2 I \end{bmatrix} \preceq 0 \quad (30)$$

$$\begin{bmatrix} \Xi & \star & \star & \star \\ D_\varepsilon^\top Y^\top & -\rho^2 I & \star & \star \\ T_m N_1 & 0 & -T_m E_1(\mathbf{h}_k) & \star \\ 3T_m N_2 & 0 & 0 & -3T_m E_1(\mathbf{h}_k) \end{bmatrix} \preceq 0 \quad (31)$$

with

$$P(\mathbf{h}_k) = \begin{bmatrix} P_1(\mathbf{h}_k) & \star \\ P_2(\mathbf{h}_k) & P_3(\mathbf{h}_k) \end{bmatrix}, \quad E(\mathbf{h}_k) = \begin{bmatrix} E_1(\mathbf{h}_k) & \star \\ E_2(\mathbf{h}_k) & E_3(\mathbf{h}_k) \end{bmatrix}$$

$$X(\mathbf{h}_k) = \begin{bmatrix} X_1(\mathbf{h}_k) & \star \\ X_2(\mathbf{h}_k) - X_1(\mathbf{h}_k) & X_1(\mathbf{h}_k) - \text{He}(X_2(\mathbf{h}_k)) \end{bmatrix}$$

$$\Xi = \Omega + T_m \Upsilon + e^{\alpha T_m} \text{He}(\Lambda \Gamma)$$

$$\Lambda^\top = [I \quad \lambda_1 I \quad \lambda_2 I \quad \lambda_3 I \quad \lambda_4 I]$$

$$\Gamma = [0 \quad 0 \quad \bar{Z} \quad 0 \quad 0], \quad \bar{Z} = \text{blkdiag}(-Z(\mathbf{h}_k)C, 0)$$

$$N_i^\top = [N_{i1}^\top \quad N_{i2}^\top \quad N_{i3}^\top \quad N_{i4}^\top \quad N_{i5}^\top], \quad i \in \mathcal{I}_2$$

$$Y^\top = [Y_1^\top \quad Y_2^\top \quad Y_3^\top \quad Y_4^\top \quad Y_5^\top]$$

$$Y_i = \begin{bmatrix} \lambda_{i-1} F(\mathbf{h}_k) & Y_{i2}(\boldsymbol{\sigma}, \mathbf{h}_k) \\ 0 & Y_{i4}(\boldsymbol{\sigma}, \mathbf{h}_k) \end{bmatrix}, \quad i \in \mathcal{I}_5 \text{ and } \lambda_0 = 1$$

$$\Omega = \text{He}(\Omega_s) + \mathbb{I}_1^\top (I + R_1 + \text{He}(P_2)) \mathbb{I}_1 - \mathbb{I}_2^\top R_1 \mathbb{I}_2$$

$$- (\mathbb{I}_1 - \mathbb{I}_2)^\top R_2 (\mathbb{I}_1 - \mathbb{I}_2) + T_m^2 \mathbb{I}_5^\top R_2 \mathbb{I}_5 - \begin{bmatrix} \mathbb{I}_1 \\ \mathbb{I}_3 \end{bmatrix}^\top X \begin{bmatrix} \mathbb{I}_1 \\ \mathbb{I}_3 \end{bmatrix}$$

$$\Omega_s = \mathbb{I}_5^\top P_1 \mathbb{I}_1 - N_1^\top (\mathbb{I}_1 - \mathbb{I}_3) - 3N_2^\top (\mathbb{I}_1 + \mathbb{I}_3 - 2\mathbb{I}_4)$$

$$- \mathbb{I}_3^\top E_2 (\mathbb{I}_1 - \mathbb{I}_3) + Y \Omega_{s1}$$

$$\Omega_{s1} = [A_\varepsilon \quad 0 \quad 0 \quad 0 \quad -I]$$

$$\Psi = \text{He}(\Psi_s) + [\mathbb{I}_5 \quad \mathbb{I}_3] E [\mathbb{I}_5 \quad \mathbb{I}_3]^\top - \mathbb{I}_4^\top Q \mathbb{I}_4 + \mathbb{I}_3^\top S \mathbb{I}_3$$

$$\Psi_s = [\mathbb{I}_5 \quad 0] X [\mathbb{I}_1 \quad \mathbb{I}_3]^\top + \mathbb{I}_1^\top Q \mathbb{I}_4$$

$$\Upsilon = \text{He}(\Upsilon_s) - \mathbb{I}_4^\top Q \mathbb{I}_4 - \mathbb{I}_3^\top (S + E_3) \mathbb{I}_3$$

$$\Upsilon_s = \mathbb{I}_1^\top P_3 \mathbb{I}_4 + \mathbb{I}_4^\top P_2 \mathbb{I}_5$$

and $\mathbb{I}_i = [0 \quad \dots \quad I \quad \dots \quad 0]$, for $i \in \mathcal{I}_5$, is an indicator vector, whose i th element is an identity matrix of suitable dimension. Then, the map from $\mathbf{w}(t)$ to $\boldsymbol{\varepsilon}(t)$ is finite \mathcal{L}_2 -gain stable such that the performance condition (25) is verified. Moreover, the observer gain is defined as

$$L(\mathbf{h}_k) = F(\mathbf{h}_k)^{-1} Z(\mathbf{h}_k). \quad (32)$$

Proof. For simplicity of notation, the dependence of all matrix variables on either $\mathbf{h}(t)$ or $\mathbf{h}(t_k)$ is dropped in the proof. Moreover, we define

$$\boldsymbol{\zeta}^\top(t) = [\boldsymbol{\varepsilon}^\top(t) \quad \boldsymbol{\varepsilon}^\top(t - T_m) \quad \boldsymbol{\varepsilon}^\top(t_k) \quad \boldsymbol{\nu}^\top(t) \quad \dot{\boldsymbol{\varepsilon}}^\top(t)]$$

with $\boldsymbol{\nu}(t) = \frac{1}{t - t_k} \int_{t_k}^t \boldsymbol{\varepsilon}(\tau) d\tau$. For stability analysis of the error dynamics (24), the following looped Lyapunov-Krasovskii function candidate is considered:

$$V(\boldsymbol{\varepsilon}) = \sum_{i=1}^5 V_i(\boldsymbol{\varepsilon}) \quad (33)$$

with

$$V_1(\boldsymbol{\varepsilon}) = \left[\int_{t_k}^t \boldsymbol{\varepsilon}(\tau) d\tau \right]^\top P \left[\int_{t_k}^t \boldsymbol{\varepsilon}(\tau) d\tau \right]$$

$$V_2(\boldsymbol{\varepsilon}) = \int_{t-T_m}^t \boldsymbol{\varepsilon}^\top(\tau) R_1 \boldsymbol{\varepsilon}(\tau) d\tau + T_m \int_{-T_m}^0 \int_{t+\theta}^t \dot{\boldsymbol{\varepsilon}}^\top(\tau) R_2 \dot{\boldsymbol{\varepsilon}}(\tau) d\tau d\theta$$

$$V_3(\boldsymbol{\varepsilon}) = (t_{k+1} - t) \int_{t_k}^t \begin{bmatrix} \dot{\boldsymbol{\varepsilon}}(\tau) \\ \boldsymbol{\varepsilon}(t_k) \end{bmatrix}^\top E \begin{bmatrix} \dot{\boldsymbol{\varepsilon}}(\tau) \\ \boldsymbol{\varepsilon}(t_k) \end{bmatrix} d\tau$$

$$V_4(\boldsymbol{\varepsilon}) = (t_{k+1} - t) \begin{bmatrix} \boldsymbol{\varepsilon}(t) \\ \boldsymbol{\varepsilon}(t_k) \end{bmatrix}^\top X \begin{bmatrix} \boldsymbol{\varepsilon}(t) \\ \boldsymbol{\varepsilon}(t_k) \end{bmatrix}$$

$$V_5(\boldsymbol{\varepsilon}) = (t_{k+1} - t)(t - t_k) (\boldsymbol{\nu}^\top(t) Q \boldsymbol{\nu}(t) + \boldsymbol{\varepsilon}^\top(t_k) S \boldsymbol{\varepsilon}(t_k)).$$

Note that the positiveness of $V(\boldsymbol{\varepsilon})$ is guaranteed by constraints (28) and (29). Taking the time derivative of each $V_i(\boldsymbol{\varepsilon})$, for $i \in \mathcal{I}_5$, we have

$$\dot{V}_1(\boldsymbol{\varepsilon}) = \text{He} \left(\boldsymbol{\zeta}^\top \begin{bmatrix} \mathbb{I}_5 \\ \mathbb{I}_1 \end{bmatrix}^\top P \begin{bmatrix} \mathbb{I}_1 \\ (t - t_k) \mathbb{I}_4 \end{bmatrix} \right) \boldsymbol{\zeta}$$

$$\dot{V}_2(\boldsymbol{\varepsilon}) = \boldsymbol{\zeta}^\top (\mathbb{I}_1^\top R_1 \mathbb{I}_1 - \mathbb{I}_2^\top R_1 \mathbb{I}_2 + T_m^2 \mathbb{I}_5^\top R_2 \mathbb{I}_5) \boldsymbol{\zeta} - T_m \int_{t-T_m}^t \dot{\boldsymbol{\varepsilon}}^\top(\tau) R_2 \dot{\boldsymbol{\varepsilon}}(\tau) d\tau$$

$$\dot{V}_3(\boldsymbol{\varepsilon}) = - \int_{t_k}^t \begin{bmatrix} \dot{\boldsymbol{\varepsilon}}(\tau) \\ \boldsymbol{\varepsilon}(t_k) \end{bmatrix}^\top E \begin{bmatrix} \dot{\boldsymbol{\varepsilon}}(\tau) \\ \boldsymbol{\varepsilon}(t_k) \end{bmatrix} d\tau$$

$$+ (t_{k+1} - t) \boldsymbol{\zeta}^\top \left(\begin{bmatrix} \mathbb{I}_5 \\ \mathbb{I}_3 \end{bmatrix}^\top E \begin{bmatrix} \mathbb{I}_5 \\ \mathbb{I}_3 \end{bmatrix} \right) \boldsymbol{\zeta} \quad (34)$$

$$\begin{aligned}
\dot{V}_4(\varepsilon) &= \zeta^\top \left(- \begin{bmatrix} \mathbb{I}_1 \\ \mathbb{I}_3 \end{bmatrix}^\top X \begin{bmatrix} \mathbb{I}_1 \\ \mathbb{I}_3 \end{bmatrix} \right. \\
&\quad \left. + (t_{k+1} - t) \text{He} \left(\begin{bmatrix} \mathbb{I}_5 \\ 0 \end{bmatrix}^\top X \begin{bmatrix} \mathbb{I}_1 \\ \mathbb{I}_3 \end{bmatrix} \right) \right) \zeta \\
\dot{V}_5(\varepsilon) &= \zeta^\top \left(- (t - t_k) \begin{bmatrix} \mathbb{I}_4 \\ \mathbb{I}_3 \end{bmatrix}^\top \begin{bmatrix} Q & 0 \\ 0 & S \end{bmatrix} \begin{bmatrix} \mathbb{I}_4 \\ \mathbb{I}_3 \end{bmatrix} \right. \\
&\quad \left. + (t_{k+1} - t) \begin{bmatrix} \mathbb{I}_4 \\ \mathbb{I}_3 \end{bmatrix}^\top \begin{bmatrix} Q & 0 \\ 0 & S \end{bmatrix} \begin{bmatrix} \mathbb{I}_4 \\ \mathbb{I}_3 \end{bmatrix} \right. \\
&\quad \left. + (t_{k+1} - t)(t - t_k) \text{He} \left(\nu^\top(t) Q \nu(t) \right) \right) \zeta.
\end{aligned}$$

Applying Jensen's inequality, see Remark 3, then $\dot{V}_2(\varepsilon)$ can be upper bounded as

$$\begin{aligned}
\dot{V}_2(\varepsilon) &\leq \zeta^\top (\mathbb{I}_1^\top R_1 \mathbb{I}_1 - \mathbb{I}_2^\top R_1 \mathbb{I}_2 + T_m^2 \mathbb{I}_5^\top R_2 \mathbb{I}_5 \\
&\quad - (\mathbb{I}_1 - \mathbb{I}_2)^\top R_2 (\mathbb{I}_1 - \mathbb{I}_2)) \zeta. \quad (35)
\end{aligned}$$

Similarly, applying Wirtinger's inequality in Lemma 2, we can prove that

$$\dot{V}_3(\varepsilon) \leq \zeta^\top \left(\Phi + (t_{k+1} - t) \begin{bmatrix} \mathbb{I}_5 \\ \mathbb{I}_3 \end{bmatrix}^\top E \begin{bmatrix} \mathbb{I}_5 \\ \mathbb{I}_3 \end{bmatrix} \right) \zeta \quad (36)$$

with

$$\begin{aligned}
\Phi &= -\frac{1}{t - t_k} \Phi_1^\top E \Phi_1 - \frac{3}{t - t_k} \Phi_2^\top E \Phi_2 \\
\Phi_1^\top &= [\mathbb{I}_1^\top - \mathbb{I}_3^\top \quad (t - t_k) \mathbb{I}_3^\top], \quad \Phi_2^\top = [\mathbb{I}_1^\top + \mathbb{I}_3^\top - 2\mathbb{I}_4^\top \quad 0].
\end{aligned}$$

Since $E \succeq 0$, it follows that

$$(E \Phi_i + (t - t_k) \bar{N}_i)^\top E^{-1} (E \Phi_i + (t - t_k) \bar{N}_i) \succeq 0 \quad (37)$$

for $i \in \mathcal{I}_2$, and with $\bar{N}_i = [\bar{N}_{i1} \quad \bar{N}_{i2} \quad \bar{N}_{i3} \quad \bar{N}_{i4} \quad \bar{N}_{i5}]$. From (36) and (37), an upper bound of $\dot{V}_3(\varepsilon)$ can be characterized as

$$\dot{V}_3(\varepsilon) \leq \zeta^\top \left(\Sigma + (t - t_k) \begin{bmatrix} \bar{N}_1^\top E^{-1} \bar{N}_1 + 3\bar{N}_2^\top E^{-1} \bar{N}_2 \end{bmatrix} \right) \zeta \quad (38)$$

with

$$\Sigma = \text{He} \left(\bar{N}_1^\top \Phi_1 + 3\bar{N}_2^\top \Phi_2 \right) + (t_{k+1} - t) \begin{bmatrix} \mathbb{I}_5 \\ \mathbb{I}_3 \end{bmatrix}^\top E \begin{bmatrix} \mathbb{I}_5 \\ \mathbb{I}_3 \end{bmatrix}.$$

Moreover, note that

$$\dot{\nu}(t) = -\frac{1}{(t - t_k)^2} \int_{t_k}^t \varepsilon(\tau) d\tau + \frac{1}{t - t_k} \varepsilon(t).$$

Then, the expression of $\dot{V}_5(\varepsilon)$ in (34) can be rewritten as

$$\begin{aligned}
\dot{V}_5(\varepsilon) &= \zeta^\top \left(- (t - t_k) \begin{bmatrix} \mathbb{I}_4 \\ \mathbb{I}_3 \end{bmatrix}^\top \begin{bmatrix} Q & 0 \\ 0 & S \end{bmatrix} \begin{bmatrix} \mathbb{I}_4 \\ \mathbb{I}_3 \end{bmatrix} \right. \\
&\quad \left. + (t_{k+1} - t) \left(\begin{bmatrix} \mathbb{I}_4 \\ \mathbb{I}_3 \end{bmatrix}^\top \begin{bmatrix} -Q & 0 \\ 0 & S \end{bmatrix} \begin{bmatrix} \mathbb{I}_4 \\ \mathbb{I}_3 \end{bmatrix} + \text{He}(\mathbb{I}_1^\top Q \mathbb{I}_4) \right) \right) \zeta. \quad (39)
\end{aligned}$$

We denote $\dot{V}(\varepsilon) = \sum_{i=1}^5 \dot{V}_i(\varepsilon)$. From (34), (35), (38) and (39), it follows that

$$\dot{V}(\varepsilon) + \|\varepsilon\|^2 - \rho^2 \|\mathbf{w}\|^2 \leq \bar{\zeta}^\top Q \bar{\zeta} \quad (40)$$

with $\bar{\zeta} = [\zeta^\top \quad \mathbf{w}^\top]^\top$, and

$$Q = \bar{\Omega} + (t - t_k) \Upsilon + (t_{k+1} - t) \Psi, \quad \bar{\Omega} = \Omega - \text{He}(Y \Omega_{s1}).$$

Note that

$$\mathcal{B} \bar{\zeta} = 0, \quad \text{with } \mathcal{B} = [A_\varepsilon \quad 0 \quad A_{\varepsilon_k} \quad 0 \quad -I \quad D_\varepsilon]. \quad (41)$$

By Finsler's lemma, we can deduce that condition $\bar{\zeta}^\top Q \bar{\zeta} \leq 0$ is verified under the algebraic constraint (41) if

$$Q + \mathcal{X} \mathcal{B} + \mathcal{B}^\top \mathcal{X}^\top \leq 0. \quad (42)$$

Then, it follows from (40) that condition (42) implies

$$\dot{V}(\varepsilon) + \|\varepsilon\|^2 - \rho^2 \|\mathbf{w}\|^2 \leq 0. \quad (43)$$

For the convexification of the observer design conditions, we select $\mathcal{X}^\top = [Y^\top \quad 0]$ while considering the expression (32). Then, we evaluate (42) at $t = t_k$, we can retrieve condition (30). Likewise, evaluating condition (42) at $t = t_{k+1}$ and performing the Schur complement lemma [37] on the terms involving E^{-1} , we can achieve condition (31).

Integrating the inequality (43) from t_0 to t , it follows that

$$V(\varepsilon) - V(\varepsilon_0) + \int_{t_0}^t \|\varepsilon(\tau)\|^2 d\tau \leq \rho^2 \int_{t_0}^t \|\mathbf{w}(\tau)\|^2 d\tau. \quad (44)$$

We distinguish the two following cases from (44).

Case 1. If $\mathbf{w}(t) = 0$, for $\forall t > 0$. It follows from (44) that $V(\varepsilon) - V(\varepsilon_0) \leq 0$. Then, based on the definition of $V(\varepsilon)$ in (33), at each sampling instant we have that

$$\lambda_{\min}(P) \|\varepsilon\|^2 \leq V(\varepsilon) \leq V(\varepsilon_0) \quad (45)$$

Considering the variable change (23), it follows from (45) that

$$\|\bar{\varepsilon}(t)\| \leq \sqrt{\frac{V(\varepsilon_0)}{\lambda_{\min}(P)}} e^{-\alpha t}$$

which, in turn, ensures Property (P1) in Problem 1.

Case 2. If $\mathbf{w}(t) \neq 0$, for $\forall t > 0$. Assuming null initial conditions, it follows from (44) that

$$V(\varepsilon) + \int_{t_0}^t \|\varepsilon(\tau)\|^2 d\tau - \rho^2 \int_{t_0}^t \|\mathbf{w}(\tau)\|^2 d\tau \leq 0. \quad (46)$$

Since $V(\varepsilon) \geq 0$, condition (46) ensures that

$$\int_{t_0}^t \|\varepsilon(\tau)\|^2 d\tau - \rho^2 \int_{t_0}^t \|\mathbf{w}(\tau)\|^2 d\tau \leq 0$$

which guarantees Property (P2) in Problem 1. \square

Remark 4. To mitigate the design conservatism, a free decision variable K of observer (9) can be considered for the optimization problem in Theorem 1. However, this directly results in a non-convex formulation with bilinear matrix inequality (BMI) constraints, posing numerical challenges in determining practical observer gains. To circumvent this issue, we adopt the matrix gain K in the specific form of (11). Notably, observe from (13) that the gain factor τ can offer flexibility for K to improve the correction of the UI estimation error.

Remark 5. Larger values of the gain factor τ in (11) and the decay rate α in (23) lead to a faster error convergence. However, this might result in aggressive estimation behaviors, such

as considerable overshoot and noise amplification. Therefore, the selection of these design parameters should ensure that the sampled-data observer, designed from Theorem 1, circumvents these practical challenges.

Remark 6. The observer design conditions in Theorem 1 are expressed in terms of LMI constraints of infinite dimension due to their dependency on \mathbf{h}_k and/or σ , which can be suitably parsed by the ROLMIP toolbox [43] generating a finite set of LMI constraints. This toolbox can also evaluate a matrix, such as (20), at the minimum and maximum of each parameter producing a convex set, which alleviates the burden of manually determining the set. The MOSEK solver is used to solve the generated LMI-based optimization problem.

IV. EXPERIMENTAL RESULTS

This section presents the experimental validation of the proposed nonlinear sampled-data observer under different test scenarios. The experiments are performed using the test facilities shown in Fig. 1. The INSA-LAMIH autonomous vehicle is equipped with a Racelogic VBOX III sensor, which includes a dual-antenna GPS system with RTK correction. Additionally, the vehicle is integrated with a 6-DoF inertial measurement unit (IMU) consisting of three accelerometers and three gyroscopes. The IMU, the dual GPS, and other measurements are processed by a fusion system. Note that as the tire forces F_{yf} and F_{yr} cannot be directly measured, these two signals are computed offline using a neural network-based inverse kinematic method and considered as ground truth values. Vehicle sensors provide measurements at 100 Hz transmitted on a single CAN bus, which is also used by other vehicle equipment. The resulting heavy CAN bus load introduces uncertainty in deterministic bus access, as sensors need to wait for bus availability. The dSpace MicroAutobox stores data from the CAN in a buffer, which is read, timestamped, and stored on disk every 10 ms. Hence, data results from asynchronous communication, timestamped with 10 ms accuracy. To handle asynchronous transmission on the CAN bus, a MASP of $T_m = 20$ ms is considered in the Host PC for analysis conducted offline as shown in Fig. 3. Consequently, for observer performance illustrations, we consider that for a sample at t_k , the next sampling time t_{k+1} can randomly occur as $t_{k+1} = t_k + T_s$, for any T_s such that $t_m \leq T_s \leq T_m$, with $t_m = 10$ ms and $T_m = 20$ ms. Note that there is no existing work on jointly estimating sideslip angle and tire-road forces under this measurement sampling condition.

Solving the optimization problem (27) in Theorem 1, we can obtain a data-sampled observer solution with $T_m = 20$, $\tau = 200$, $\alpha = 50$, $\lambda_4 = 1$, $\lambda_i = 0$, for $i \in \mathcal{I}_3$, an \mathcal{L}_2 -gain bound of $\rho = 4.5 \times 10^{-3}$. For comparison, we assess three nonlinear observers using the same gain expression (32):

- SDO: Proposed sampled-data observer.
- DO10 and DO20: Two discrete-time observers with a *periodic* (fixed) sampling time of 10 ms and 20 ms, respectively.

The synthesis of the two observers, DO10 and DO20, is based on the assumption of fixed sampling times of 10 ms and 20 ms, respectively, corresponding to the minimum and maximum allowable sampling periods. For brevity, the

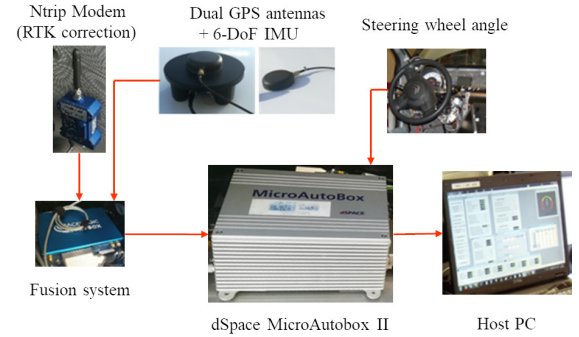


Fig. 3. Vehicle embedded acquisition system with onboard sensors.

discrete-time observer design and all obtained solutions are not reported here. Nevertheless, these details are provided in the supplementary material available at <https://bitly.ws/3b5Ug>. The practical performance of the three considered observers is validated under three test scenarios: (i) random smooth driving with a roundabout, (ii) sharp turn, and (iii) extreme driving conditions. Note that, for better graphical illustrations, we only show the estimation performance of two observers, SDO and DO10. As expected, the latter exhibits better performance than DO20, as will be quantitatively compared later.

A. Test 1: Normal Driving with a Roundabout

During this test, the vehicle is maneuvered along a trajectory, encompassing gentle turns and a circular intersection, as shown in Fig. 4(a). The longitudinal speed, the steering angle, and the wheel torque corresponding to this scenario are presented in Figs. 4(b), (c) and (d). The estimation results are depicted in Fig. 5. We remark that both SDO and DO10 observers deliver excellent estimates of the lateral speed. While the DO10 observer can provide a good estimation of the road-tire forces, the proposed SDO observer still demonstrates better performance when driving throughout the track.

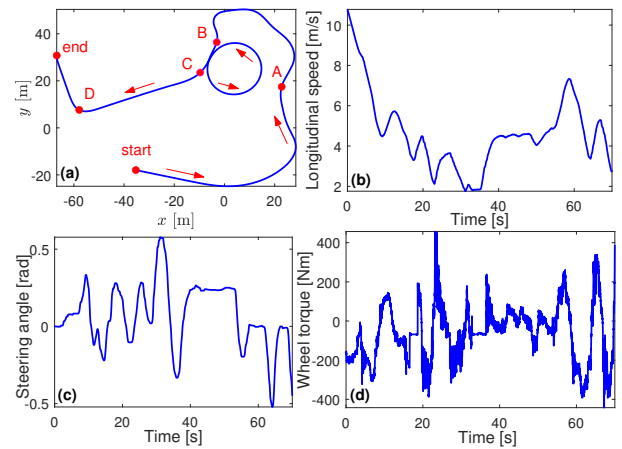


Fig. 4. Test 1. (a) Vehicle trajectory, (b) Vehicle longitudinal speed v_x , (c) Steering angle δ , (d) Wheel torque T_w .

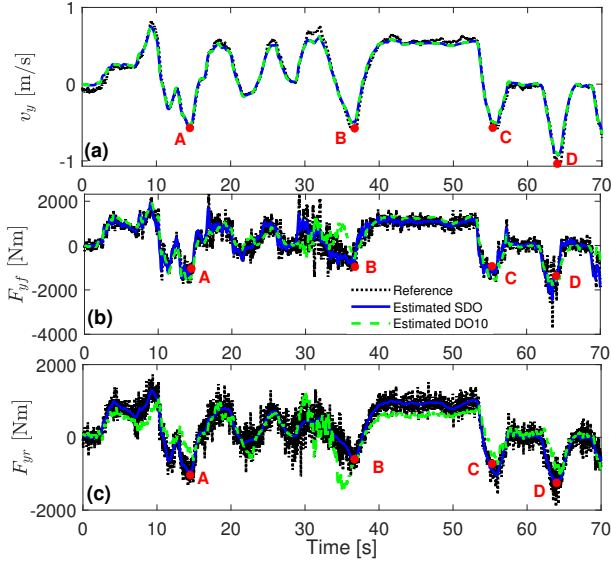


Fig. 5. Estimation performance obtained with Test 1. (a) Lateral speed v_y , (b) Lateral force on front tires F_{yf} , (c) Lateral force on rear tires F_{yr} .

B. Test 2: Driving with Sharp Turns

In this test scenario, the vehicle performs three sharp turns at points A, B and C as depicted in Fig. 6(a), and then is smoothly driven through the track. The corresponding vehicle trajectory, the time-varying longitudinal speed, the steering angle, and the wheel torque are presented in Fig. 6. Fig. 7 shows that the unmeasured lateral speed, as well as the tire-road forces, are precisely estimated with the proposed SDO observer despite the sharp turns. The estimates of the road-tire forces given by the DO10 observer are much less accurate than those of the SDO observer since *asynchronous* sensor measurements were not considered in its design.

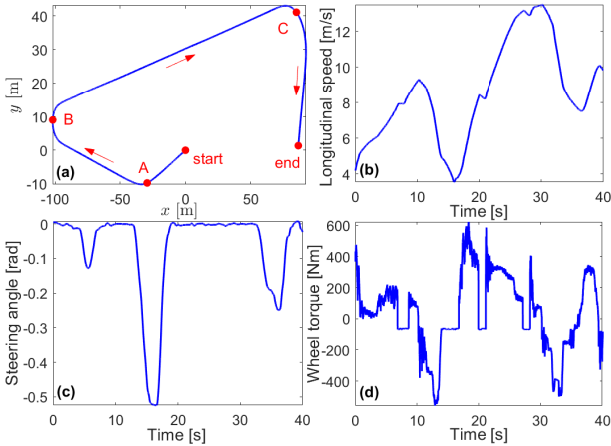


Fig. 6. Test 2. (a) Vehicle trajectory, (b) Vehicle longitudinal speed v_x , (c) Steering angle δ , (d) Wheel torque T_w .

C. Test 3: Driving under Extreme Conditions

This test is performed with a challenging driving situation, where the vehicle is driven with some *zigzag* behaviors. The corresponding vehicle trajectory, the time-varying speed, the

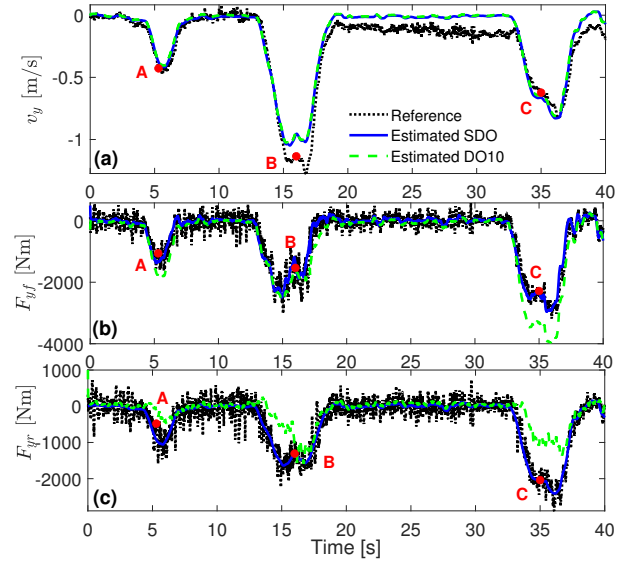


Fig. 7. Estimation performance obtained with Test 2. (a) Lateral speed v_y , (b) Lateral force on front tires F_{yf} , (c) Lateral force on rear tires F_{yr} .

steering angle and the wheel torque are shown in Fig. 8. The aggressive driving style leads to a longitudinal speed profile characterized by rapid shifts in both steering angle and lateral speed, as illustrated in Figs. 8(b), (c), and Fig. 9(a), respectively. In specific segments of the test, notably from 2 s to 6 s, the estimation performance of lateral speed is not satisfactory. This is primarily due to violent zigzag driving patterns performed by the driver on straight road sections, as seen in Fig. 8. The simplified vehicle model (1) fails to effectively capture the highly solicited nonlinear dynamics in this scenario, leading to a degradation in the performance of the considered model-based observers. However, despite this challenging test, the proposed sampled-data observer is still able to accurately estimate the unmeasured variables v_y , F_{yf} , and F_{yr} , especially during sharp turns and sudden changes of direction, as shown in Fig. 9. Similarly to the two previous tests, although both SDO and DO10 observers exhibit similar performance for lateral speed estimation, the SDO observer demonstrates significantly better accuracy in estimating road-tire forces.

For a quantitative estimation performance analysis, the root mean square errors (RMSE) and mean absolute errors (MAE) of the unmeasured lateral speed v_{yRMSE} and v_{yMAE} , the lateral road-tire forces F_{yfRMSE} and F_{yfMAE} , and F_{yrRMSE} and F_{yrMAE} , obtained with the three considered nonlinear observers (SDO, DO10 and DO20), are computed. These performance indicators are summarized in Table II for the three driving scenarios. First, the numerical results confirm that all three observers provide good estimates of the lateral speed, even though the performance of the DO20 observer is significantly more degraded under extreme driving conditions in Test 3. Second, the error indicators related to the road-tire forces seem to be higher than expected, primarily caused by measurement outliers, as shown in Figs. 5, 7 and 9. However, from a global perspective, we observe that the SDO observer outperforms the DO10 observer, which, in turn, provides better

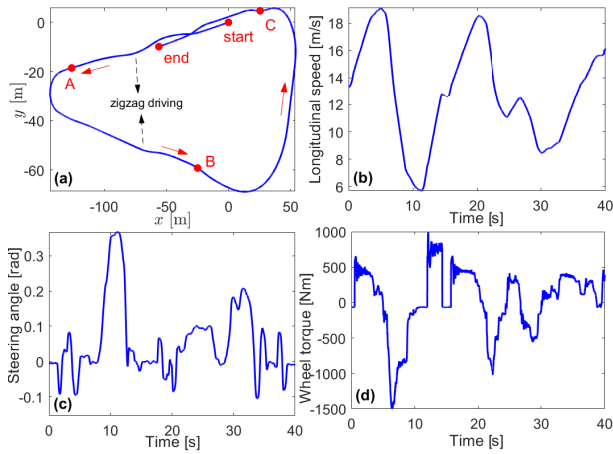


Fig. 8. Test 3. (a) Vehicle trajectory, (b) Vehicle longitudinal speed v_x , (c) Steering angle δ , (d) Wheel torque T_w .

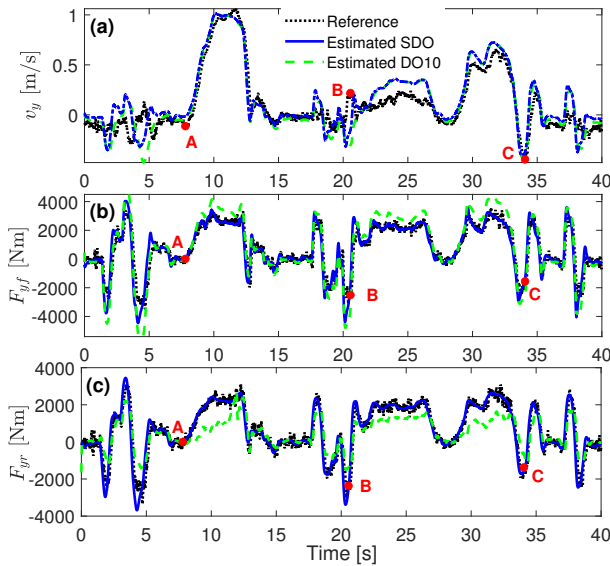


Fig. 9. Estimation performance obtained with Test 3. (a) Lateral speed v_y , (b) Lateral force on front tires F_{yf} , (c) Lateral force on rear tires F_{yr} .

estimation quality compared to the DO20. Third, the analysis results confirm that the proposed SDO observer consistently achieves a highly satisfactory estimation performance under all considered test scenarios.

V. CONCLUSIONS AND FUTURE WORKS

A nonlinear data-sampled observer design has been proposed to jointly estimate the sideslip angle and the lateral road-tire forces of autonomous ground vehicles. To this end, we develop a nonlinear observer, which is able to reconstruct both the vehicle state and the unknown input without requiring the well-known matching condition. In particular, we consider sampled vehicle measurements, which can practically take place at arbitrary instants in a certain window with upper and lower limits. To derive the observer design conditions, the nonlinear estimation error dynamics is parameterized in an LPV polytopic form. Then, Lyapunov-Krasovskii stability theory is leveraged to ensure the exponential error convergence

while guaranteeing a maximum allowable sampling period and an \mathcal{L}_2 -gain performance. The data-sampled observer design is recast as an LMI-based optimization problem, which can be efficiently resolved using common numerical solvers. The practical estimation performance of the new nonlinear data-sampled observer is experimentally validated under representative test scenarios. The experimental results show that the proposed method can provide accurate estimates of both the sideslip angle and the lateral road-tire forces.

It is challenging to fully capture the nonlinearities of tire forces using uncertain linear models, as shown in (4), especially under limit handling conditions. Future work will focus on using more accurate tire force models, such as nonlinear or piecewise affine models, for observer design to improve estimation performance, especially under limit handling conditions. Another future research direction is to exploit the proposed estimation method to design an effective fault-tolerant control scheme for autonomous vehicles under on-the-limit driving situations.

REFERENCES

- [1] X. Ding, Z. Wang, L. Zhang, and J. Liu, "A comprehensive vehicle stability assessment system based on enabling tire force estimation," *IEEE Trans. Veh. Technol.*, vol. 71, no. 11, pp. 11 571–11 588, 2022.
- [2] B. Singh, A. Arat, and S. Taheri, "Literature review and fundamental approaches for vehicle and tire state estimation," *Veh. Syst. Dyn.*, vol. 57, no. 11, pp. 1643–1665, 2019.
- [3] S. Yang, Y. Chen, R. Shi, R. Wang, Y. Cao, and J. Lu, "A survey of intelligent tires for tire-road interaction recognition toward autonomous vehicles," *IEEE Trans. Intell. Veh.*, vol. 7, no. 3, pp. 520–532, 2022.
- [4] Z. Wang, X. Zhou, and J. Wang, "Extremum-seeking-based adaptive model-free control and its application to automated vehicle path tracking," *IEEE/ASME Trans. Mechatron.*, vol. 27, no. 5, pp. 874–884, 2022.
- [5] H. Guo, Z. Yin, D. Cao, H. Chen, and C. Lv, "A review of estimation for vehicle tire-road interactions toward automated driving," *IEEE Trans. Syst., Man, Cybern.: Syst.*, vol. 49, no. 1, pp. 14–30, 2018.
- [6] S. Cheng, L. Li, B. Yan, C. Liu, X. Wang, and J. Fang, "Simultaneous estimation of tire side-slip angle and lateral tire force for vehicle lateral stability control," *Mech. Syst. Signal Process.*, vol. 132, pp. 68–82, 2019.
- [7] Z. Zou, X. Zhang, Y. Zou, and B. Lenzo, "Tire-road friction coefficient estimation method design for intelligent tires equipped with three-axis accelerometer," *SAE Int. J. Veh. Dyn., Stab., and NVH*, vol. 5, no. 10-05-03-0017, pp. 249–258, 2021.
- [8] A. Borri, "A nonlinear sampled-data observer of vehicle lateral velocity," *IEEE Control Syst. Lett.*, vol. 1, no. 2, pp. 244–249, 2017.
- [9] A.-T. Nguyen, T. Dinh, T.-M. Guerra, and J. Pan, "Takagi–Sugeno fuzzy unknown input observers to estimate nonlinear dynamics of autonomous ground vehicles: Theory and real-time verification," *IEEE/ASME Trans. Mechatron.*, vol. 26, no. 3, pp. 1328–1338, 2021.
- [10] Y. Wang, K. Geng, L. Xu, Y. Ren, H. Dong, and G. Yin, "Estimation of sideslip angle and tire cornering stiffness using fuzzy adaptive robust cubature Kalman filter," *IEEE Trans. Syst., Man, Cybern.: Syst.*, vol. 52, no. 3, pp. 1451–1462, 2020.
- [11] L.-H. Zhao, Z.-Y. Liu, and H. Chen, "Design of a nonlinear observer for vehicle velocity estimation and experiments," *IEEE Trans. Control Syst. Technol.*, vol. 19, no. 3, pp. 664–672, 2010.
- [12] C. Ahn, H. Peng, and E. Tseng, "Robust estimation of road friction coefficient," *IEEE Trans. Cont. Syst. Tech.*, vol. 2, no. 1, pp. 1–13, 2013.
- [13] Y.-H. Liu, T. Li, Y.-Y. Yang, X.-W. Ji, and J. Wu, "Estimation of tire-road friction coefficient based on combined APF-IEKF and iteration algorithm," *Mech. Syst. Signal Process.*, vol. 88, pp. 25–35, 2017.
- [14] Z. Zhang, L. Zheng, H. Wu, Z. Zhang, Y. Li, and Y. Liang, "An estimation scheme of road friction coefficient based on novel tyre model and improved SCKF," *Veh. Syst. Dyn.*, vol. 60, no. 8, pp. 775–804, 2022.
- [15] J. Villagra, B. D'Andréa-Novel, M. Fliess, and H. Mounier, "A diagnosis-based approach for tire-road forces and maximum friction estimation," *Control Eng. Pract.*, vol. 19, no. 2, pp. 174–184, 2011.
- [16] B. Zhang, H. Du, J. Lam, N. Zhang, and W. Li, "A novel observer design for simultaneous estimation of vehicle steering angle and sideslip angle," *IEEE Trans. Indus. Electron.*, vol. 63, no. 7, pp. 4357–4366, 2016.

TABLE II
QUANTITATIVE ESTIMATION PERFORMANCE OF ALL TEST SCENARIOS.

Error indicator	Scenario 1			Scenario 2			Scenario 3		
	SDO	DO10	DO20	SDO	DO10	DO20	SDO	DO10	DO20
v_{yRMSE} [m/s]	0.05	0.06	0.07	0.09	0.10	0.11	0.13	0.14	0.29
F_{yfRMSE} [Nm]	303.41	453.98	604.69	237.12	400.18	459.02	669.93	779.86	821.36
F_{yrRMSE} [Nm]	217.35	391.38	2707.23	225.76	488.22	934.03	473.52	687.27	1554.14
v_{yMAE} [m/s]	0.04	0.05	0.053	0.08	0.08	0.09	0.10	0.11	0.21
F_{yfMAE} [Nm]	215.02	307.54	453.69	177.97	275.19	306.56	435.45	591.95	624.12
F_{yrMAE} [Nm]	166.81	301.97	1262.25	174.03	330.17	531.43	304.30	535.55	1179.74

- [17] S. Han and K. Huh, "Monitoring system design for lateral vehicle motion," *IEEE Trans. Veh. Technol.*, vol. 60, no. 4, pp. 1394–1403, 2011.
- [18] M. Doumiati, C. Victorino, A. Charara, and D. Lechner, "Onboard real-time estimation of vehicle lateral tire–road forces and sideslip angle," *IEEE/ASME Trans. Mechatron.*, vol. 16, no. 4, pp. 601–614, 2010.
- [19] D. Jeong, G. Ko, and S. Choi, "Estimation of sideslip angle and cornering stiffness of an articulated vehicle using a constrained lateral dynamics model," *Mechatronics*, vol. 85, p. 102810, 2022.
- [20] H. Guo, H. Chen, F. Xu, F. Wang, and G. Lu, "Implementation of EKF for vehicle velocities estimation on FPGA," *IEEE Trans. Indus. Electron.*, vol. 60, no. 9, pp. 3823–3835, 2012.
- [21] M. Gadola, D. Chindamo, M. Romano, and F. Padula, "Development and validation of a Kalman filter-based model for vehicle slip angle estimation," *Veh. Syst. Dyn.*, vol. 52, no. 1, pp. 68–84, 2014.
- [22] S. Cheng, L. Li, and J. Chen, "Fusion algorithm design based on adaptive SCKF and integral correction for side-slip angle observation," *IEEE Trans. Indus. Electron.*, vol. 65, no. 7, pp. 5754–5763, 2017.
- [23] Y. Wang, L. Xu, F. Zhang, H. Dong, Y. Liu, and G. Yin, "An adaptive fault-tolerant EKF for vehicle state estimation with partial missing measurements," *IEEE/ASME Trans. Mechatron.*, vol. 26, no. 3, pp. 1318–1327, 2021.
- [24] K. Zhang, Y. Zhang, and P. Xu, "An algorithm for parameter identification of semi-empirical tire model," *SAE Int. J. Veh. Dyn., Stab., and NVH*, vol. 5, no. 10-05-03-0026, pp. 379–396, 2021.
- [25] L. Bascetta and G. Ferretti, "LFT-based identification of lateral vehicle dynamics," *IEEE Technol.*, vol. 71, no. 2, pp. 349–362, 2022.
- [26] S. Strano and M. Terzo, "Constrained nonlinear filter for vehicle sideslip angle estimation withno a priori knowledge of tyre characteristics," *Control Eng. Pract.*, vol. 71, pp. 10–17, 2018.
- [27] E. Joa, K. Yi, and Y. Hyun, "Estimation of the tire slip angle under various road conditions without tire–road information for vehicle stability control," *Control Eng. Pract.*, vol. 86, pp. 129–143, 2019.
- [28] N. Xu, Y. Huang, H. Askari, and Z. Tang, "Tire slip angle estimation based on the intelligent tire technology," *IEEE Trans. Veh. Technol.*, vol. 70, no. 3, pp. 2239–2249, 2021.
- [29] C. Nguyen, A.-T. Nguyen, and S. Delprat, "Neural-network-based fuzzy observer with data-driven uncertainty identification for vehicle dynamics estimation under extreme driving conditions: Theory and experimental results," *IEEE Trans. Veh. Technol.*, vol. 72, no. 7, pp. 8686–8696, 2023.
- [30] M. Viehweger, C. Vasseur, S. van Aalst, M. Acosta, E. Regolin, A. Alatorre, W. Desmet, F. Naets, V. Ivanov, A. Ferrara *et al.*, "Vehicle state and tyre force estimation: Demonstrations and guidelines," *Veh. Syst. Dyn.*, vol. 59, no. 5, pp. 675–702, 2021.
- [31] W. Liu, X. Xia, L. Xiong, Y. Lu, L. Gao, and Z. Yu, "Automated vehicle sideslip angle estimation considering signal measurement characteristic," *IEEE Sensors J.*, vol. 21, no. 19, pp. 21 675–21 687, 2021.
- [32] W. Jeon, A. Zemouche, and R. Rajamani, "Tracking of vehicle motion on highways and urban roads using a nonlinear observer," *IEEE/ASME Trans. Mechatron.*, vol. 24, no. 2, pp. 644–655, 2019.
- [33] J. Pan, A.-T. Nguyen, T.-M. Guerra, C. Sentouh, S. Wang, and J.-C. Popieul, "Vehicle actuator fault detection with finite-frequency specifications via Takagi-Sugeno fuzzy observers: Theory and experiments," *IEEE Trans. Veh. Technol.*, vol. 72, no. 1, pp. 407–417, 2023.
- [34] H. Ren, H. Karimi, R. Lu, and Y. Wu, "Synchronization of network systems via aperiodic sampled-data control with constant delay and application to unmanned ground vehicles," *IEEE Trans. Indus. Electron.*, vol. 67, no. 6, pp. 4980–4990, 2020.
- [35] L. Hetel, C. Fiter, H. Omran, A. Seuret, E. Fridman, J.-P. Richard, and S. Niculescu, "Recent developments on the stability of systems with aperiodic sampling," *Automatica*, vol. 76, pp. 309–335, 2017.
- [36] I. Karafyllis and C. Kravaris, "From continuous-time design to sampled-data design of observers," *IEEE Trans. Autom. Control*, vol. 54, no. 9, pp. 2169–2174, 2009.
- [37] S. Boyd, L. El Ghaoui, E. Feron, and V. Balakrishnan, *Linear Matrix Inequalities in System and Control Theory*. Philadelphia, PA: SIAM, 1994, vol. 15.
- [38] R. Rajamani, *Vehicle Dynamics and Control*. Springer Science & Business Media, 2011.
- [39] Q. Jia, W. Chen, Y. Zhang, and H. Li, "Fault reconstruction and fault-tolerant control via learning observers in Takagi–Sugeno fuzzy descriptor systems with time delays," *IEEE Trans. Indus. Electron.*, vol. 62, no. 6, pp. 3885–3895, 2015.
- [40] A.-T. Nguyen, C. Sentouh, and J.-C. Popieul, "Driver-automation cooperative approach for shared steering control under multiple system constraints: Design and experiments," *IEEE Trans. Indus. Electron.*, vol. 64, no. 5, pp. 3819–3830, 2017.
- [41] K. Tanaka and H. Wang, *Fuzzy Control Systems Design and Analysis: a Linear Matrix Inequality Approach*. John Wiley & Sons, 2004.
- [42] A. Seuret and F. Gouaisbaut, "Wirtinger-based integral inequality: Application to time-delay systems," *Automatica*, vol. 49, no. 9, pp. 2860–2866, 2013.
- [43] C. Agulhari, A. Felipe, R. Oliveira, and P. Peres, "Algorithm 998: The Robust LMI Parser—A toolbox to construct LMI conditions for uncertain systems," *ACM Trans. Math. Softw.*, vol. 45, no. 3, pp. 1–25, 2019.



Anh-Tu Nguyen (M'18, SM'21) is an Associate Professor at the INSA Hauts-de-France, Université Polytechnique Hauts-de-France, Valenciennes, France. He is an Associate Editor for several top-level international journals, including IEEE/ASME TMECH, IEEE T-ITS, IFAC CEP, ISA Transactions. His research interests include robust control and estimation with mechatronics applications.



Luciano Frezzatto received his Ph.D. degree in Electrical Engineering from University of Campinas, Brazil, in 2009, 2011 and 2017, respectively. He is a Professor at the Universidade Federal de Minas Gerais, Brazil. His research interests include LPV control theory and applications.



Thierry-Marie Guerra is a Full Professor at Université Polytechnique Hauts-de-France, France. He received his PhD degree in automatic control in 1991 and the HDR in 1999. He is an Associate Editor for IEEE TFS and FSS. His major research interests include Takagi-Sugeno control and observation with applications to mobility and disabled persons.



Sébastien Delprat received the Ph.D. degree in 2002 from the University of Valenciennes, France. Since 2012, he has been a Full Professor. He is an Associate Editor of IEEE Transactions on Vehicular Technology. His research interests include vehicle control and vehicle energy management.